

F. Souris · J. Grucker · J. Dupont-Roc ·
Ph. Jacquier

Investigating metastable hcp solid helium below its melting pressure

12.06.2010

Keywords quantum solids, hcp solid helium, metastability, vacancy

Abstract We report a first attempt to produce metastable hcp solid helium below its melting pressure. A focused sound pulse is emitted along the c -axis of a mono-domain hcp helium-4 crystal starting from a static pressure just above the melting pressure. The sound pulse is made as simple as possible with one negative and one positive swing only. Density at focus is monitored by an optical interferometric method. Performed numerical simulations show that the crystal anisotropy splits the focused wave into two separate pulses, corresponding to a longitudinal wave along the c -axis and a radial one perpendicular to it. The amplification factor due to focusing remains nevertheless important. Negative pressure swings up to 0.9 bar have been produced, crossing the static melting pressure limit. Improvements in the detection method and in the focusing amplification are proposed.

PACS numbers: 67.80.B-, 67.80.bd, 64.70D-, 62.30.+d

1 Introduction

The hcp solid phase for helium-4 is stable only above a minimum pressure $P_f(T) \simeq 25$ bar at low temperature. Recently it has been suggested¹ that this solid phase remains metastable at much lower pressures. Based on an extrapolation of the equation of state, the spinodal line is predicted to be at negative pressure, about -10 bar. Beside testing this prediction, there is another interest to investigate solid helium at pressures below the melting pressure. Vacancies in this quantum solid have been studied for a long time. In particular their energy E_v has been measured

Laboratoire Kastler Brossel, ENS/CNRS/Université Paris 6,
24 rue Lhomond
Paris, F75005, France
Tel.:331 44323421
Fax:331 44323434
E-mail: fabien.souris@lkb.ens.fr

at different pressures², and also computed by Quantum Monte Carlo simulations³. Although there is a significant scatter on the measured values of E_v , it is striking that it is a strongly decreasing function of the molar volume V_m . A simple linear extrapolation on the data gathered in reference² suggests that an increase of V_m by only 5% beyond the melting volume could bring E_v near zero. Although this is a large increase for a condensed phase, this is not so for solid helium which is a very compressible material. More precisely, the maximum molar volume for stable hcp helium-4⁴ is $V_f = 21 \text{ cm}^3$, the aimed value is $V_a = 22 \text{ cm}^3$, while the predicted value of V_m at the spinodal line is $V_s = 34.7 \text{ cm}^3$. Hence V_a is within a possibly accessible range. If so, this would bring interesting new physics for solid helium. With E_v near zero, vacancies could proliferate, reach a sizable population, possibly undergo a Bose-Einstein condensation, thus realizing the Andreev scenario for supersolidity⁵. Or if the vacancy-vacancy interaction is strong enough^{3,6}, it could provide another mechanism for destabilizing the solid phase before reaching V_s .

Many different methods have been used to study metastable condensed phases, mostly liquid, under depression⁷. Metastability cannot be easily obtained for a solid because the interfaces between a solid and the container walls are disordered, and generally nucleates the liquid phase. Focused sound waves provide a way to circumvent this difficulty. Starting from a pressure P_0 above P_f , a sound pulse with an amplitude δP_i smaller than $P_0 - P_f$ at the surface of the transducer will not bring the solid below the melting pressure at the transducer surface. On its propagation to the focus the sound pressure can be amplified by a large amount, namely $\Omega R/\lambda_s$ (Ω , solid angle of the sound beam, R transducer radius, λ_s sound wavelength). Hence the peak pressure $P_0 + \delta P_i \Omega R/\lambda_s$ can explore the metastable domain below P_f with negative δP_i .

This article reports a first attempt to produce metastable hcp solid helium below its melting pressure. A hemispherical transducer was used to produce a converging sound wave. The density variations at focus are monitored by an optical interferometric method. The experimental arrangement is described in section 2. Because the sound velocity is anisotropic, the focusing is not expected to be perfect in hcp helium. A numerical simulation was made to model the remaining amplification in this case and to determine the relation between the optical signal and the density at focus. Numerical predictions are discussed in section 3. Experimental results are reported and discussed in section 4. Possible improvements and conclusions are given in section 5.

2 Experimental arrangement and procedure

The experimental cell is a 4 cm stainless steel cube, with five silica windows (diam. 2.5 cm), cooled from the top by a pumped helium-4 fridge in the 1.0-1.4 K temperature range. To achieve single crystal growth, the nucleation and growth is made at constant temperature and pressure (1.2 K and 25.5 bar). An electro-crystallization device⁸ provides a unique seed which falls on the bottom of the cell. The crystal is subsequently grown from this seed. The orientation of the c -facet (most often horizontal) is easily monitored visually during the growth process which takes place below the corresponding roughening transition 1.3 K⁹.

A hemispherical piezoelectric transducer of 6 mm internal radius (from Channel Industries) is suspended above the middle of the cell with its axis vertical,

along the crystal c -axis. Such a transducer has two main resonant modes: the thickness mode frequency is $\nu_{hf} \simeq 1$ MHz, the inner and outer surfaces vibrating in opposite directions. The breathing mode corresponds to an oscillation of the transducer radius and has a frequency $\nu_{lf} \simeq 180$ kHz. In order to simplify as much as possible the pressure wave, a single oscillation of the thickness mode was used. The driving voltage is produced by an arbitrary function generator and amplified by a RF amplifier up to a voltage ranging from 100 V to 800 V on 50 Ω . The pulse shape is designed to leave the transducer at rest at the end of the pulse. Beside the one-cycle oscillation at 1 MHz, the exciting pulse also produces a parasitic oscillation of the low frequency breathing mode which appears after the end of the 1 MHz pulse. The sound velocity in hcp solid helium is anisotropic. For longitudinal waves, the velocity is about 540 m/s along the c -axis and 460 m/s when the wave vector is in the basal plane¹⁰. Hence the initially spherical wave does not remain so and breaks up into two parts: one along the c -axis, named as ‘ z -pulse’ hereafter, and another radial one, named ‘ r -pulse’. Both show a maximum amplitude near the center of the transducer. Their relative intensity and shape will be discussed in the next section. In order to have an optical access to the transducer center two small notches (1 mm wide, 1.5 mm high) were made on the transducer rim, along a diameter.

The phenomena at the focus are monitored optically. A CW-laser beam ($\lambda_o = 532$ nm) propagating along the y -axis is focused at the cell center with a 30 μ m waist. The laser polarization is along the vertical z -axis. The axis origin is taken at the transducer center. Density modulations along the beam path produced by the sound wave result in an optical phase change

$$\delta\phi(x, z) = \frac{2\pi}{\lambda_o} \int_{-l/2}^{l/2} dy \delta n(\sqrt{x^2 + y^2}, z) \quad (1)$$

where l is the cell length. The change in refractive index δn is related to that of density $\delta\rho$ through $\delta n/(n-1) = \delta\rho/\rho$. This linear approximation of the Clausius-Mossotti relation holds for helium with a relative error less than 10^{-4} for $\delta\rho/\rho$ up to 0.1, well beyond the strains discussed here (less than 10^{-2}). Because of the system cylindrical symmetry around the z -axis, δn and $\delta\rho$ only depend on $r = \sqrt{x^2 + y^2}$ and z . To measure $\delta\phi(t)$, the laser beam is split before the cell to produce a reference beam which crosses the cell in an unperturbed region and is recombined with the monitoring beam on a photo-detector, making a Jamin interferometer. $\delta\phi(t)$ contains a low frequency part $\delta\phi_{lf}(t)$ due to the transducer breathing mode (at ν_{lf}), and the interesting signal $\delta\phi_{hf}(t)$ due to the thickness oscillation (at ν_{hf}). To extract the latter from $\delta\phi(t)$, a model of the low frequency signal $As_{lf}(t-t_0)$ has been constructed with two adjustable parameters: its amplitude A and its starting time t_0 . These parameters are determined from a fit of $As_{lf}(t-t_0)$ to $\delta\phi(t)$ filtered with a low-pass filter. Then $\delta\phi_{hf}(t)$ is found as $\delta\phi_{hf}(t) = \delta\phi(t) - As_{lf}(t-t_0)$.

Extracting $\delta n(t)$ from $\delta\phi_{hf}(t)$ is more involved. This amounts to determine a characteristic length a of the focused sound wave such that

$$\delta\phi_{hf}(t, 0, 0) = 2\pi\delta n(t, 0, 0)a/\lambda_o. \quad (2)$$

For a continuous sinusoidal wave, $a = \lambda_s/2$ ¹². There are two ways to get a . If one can measure $\delta\phi_{hf}(t, x, 0)$ for the whole range of x where it is non-zero, one can

invert formula 1 and get $\delta n(t, x, 0)$ from $\delta \phi_{hf}(t, x, 0)$ by an inverse Abel transform. This is not always possible however due to the small width of the notch. A simpler method relies on numerical simulation to get the ratio $\delta \phi_{hf}(t, 0, 0)/n(t, 0, 0)$ and thus a . In the following, results are discussed using the optical length variations $\delta L_{\text{opt}} = \lambda_o \delta \phi_{hf}/(2\pi)$ as the signal instead of $\delta \phi_{hf}$.

3 Numerical simulation of a focused spherical sound wave

Since solid helium has a close-packed hexagonal structure (hcp), its linear elastic properties are described by five elastic constants, c_{11} , c_{12} , c_{13} , c_{33} , c_{44} as defined by Musgrave¹³. The ratio of shear stress to shear strain in the meridian plane, called c_{55} is not an independent constant in hcp crystals¹⁴ and is equal to $(c_{11} - c_{12})/2$. Numerical values of the c_{ij} have been taken from¹⁵: $c_{11}/\rho = 21.2$, $c_{12}/\rho = 11.1$, $c_{13}/\rho = 5.49$, $c_{33}/\rho = 29.0$, and $c_{44}/\rho = 6.52$, all in units of 10^4 (m/s)².

The axis of the transducer being parallel to the c -axis of the crystal, deformations are of cylindrical symmetry. Elastic waves are thus governed by two coupled second order differential equations for the only two possible components of the displacement vector, u_r and u_z :

$$\rho \ddot{u}_r = c_{11} \left(\frac{\partial^2 u_r}{\partial r^2} + \frac{1}{r} \frac{\partial u_r}{\partial r} - \frac{u_r}{r^2} \right) + (c_{13} + c_{55}) \frac{\partial^2 u_z}{\partial r \partial z} + c_{55} \frac{\partial^2 u_r}{\partial z^2} \quad (3)$$

$$\rho \ddot{u}_z = (c_{13} + c_{55}) \left(\frac{\partial^2 u_r}{\partial r \partial z} + \frac{1}{r} \frac{\partial u_r}{\partial z} \right) + c_{33} \frac{\partial^2 u_z}{\partial z^2} + c_{55} \left(\frac{\partial^2 u_z}{\partial r^2} + \frac{1}{r} \frac{\partial u_z}{\partial r} \right) \quad (4)$$

(c_{44} plays no role in this geometry)

Special care must be taken in $r = 0$: for symmetry reasons, u_r , \dot{u}_r and \ddot{u}_r must be 0 in $r = 0$. Using the l'Hospital's rule, equation 4 can be rewritten:

$$\rho \ddot{u}_z = 2(c_{13} + c_{55}) \frac{\partial^2 u_r}{\partial r \partial z} + c_{33} \frac{\partial^2 u_z}{\partial z^2} + 2c_{55} \frac{\partial^2 u_z}{\partial r^2} \quad (r = 0) \quad (5)$$

These equations are integrated using a finite difference method and a staggered leap frog scheme with initial conditions corresponding to an undeformed crystal at rest. The model volume is $0 \leq r \leq 7.5$ and $-7.5 \leq z \leq 7.5$ (in mm) and is discretized on a 1024×2048 grid. The spatial step δl is then small enough compared to the wavelength ($\lambda_s \simeq 0.5$ mm) that the dispersion introduced by the discretization is negligible. The time step δt is taken to be sufficiently small to fulfill the Courant criterion: essentially one must have $\delta l / \delta t < \lambda_s v_{hf}$. At each time step t one then calculates a new field of displacement vectors with the help of the above mentioned differential equations as a function of the fields at time $t - \delta t$ and $t - 2\delta t$. The field is then adjusted so as to fulfill the boundary conditions: u_r and u_z are forced to be that of the transducer on the points belonging to it and $u_z(r = 0, z)$ is adjusted to the value $u_z(0, z) = (4u_z(\delta l, z) - u_z(2\delta l, z))/3$ to ensure cancelation of its derivative $\frac{\partial u_z}{\partial r}(r = 0, z)$. The other boundaries are left free, giving rise to reflected waves, which arrive at the focus with a long enough delay to be of no concern. From the displacement vector field, the change in molar volume can be computed ($\delta V_m / V_m = \frac{\partial u_r}{\partial r} + \frac{u_r}{r} + \frac{\partial u_z}{\partial z}$) and thus the change in refractive index

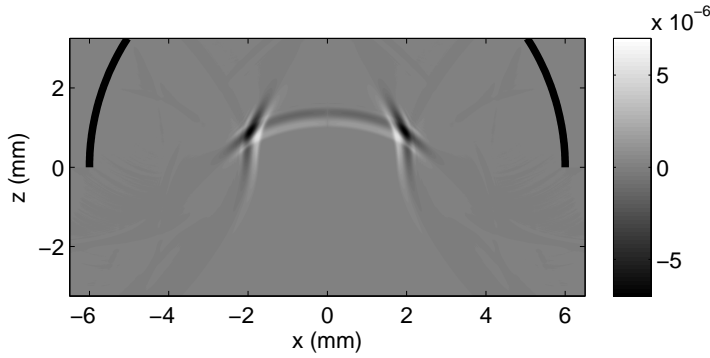


Fig. 1 Map in the zx -plane of the refractive index variations while the mono-oscillation sound wave is propagating. The thick black line represents the section of the transducer surface. The initially hemispherical wave splits into an axial wave and a radial one.

δn . An example of the wave resulting of a single oscillation of the transducer is shown on Figure 1 at time $t = 9 \mu\text{s}$. As expected, the wave has split into two parts, one along the z -axis and a slower one which becomes almost cylindrical, traveling roughly in the r direction. At the center one thus expects two pulses, as confirmed by Figure 2-a. When passing through the center, the r -wave undergoes a Gouy phase reversal. As a result the r -pulse is tripolar instead of being bipolar like the z -pulse. Note that this is true only at the center, because only at the center does the incoming and the outgoing waves interfere. An important result is the amplification factor. The z -pulse is almost not amplified, while the r -pulse is amplified

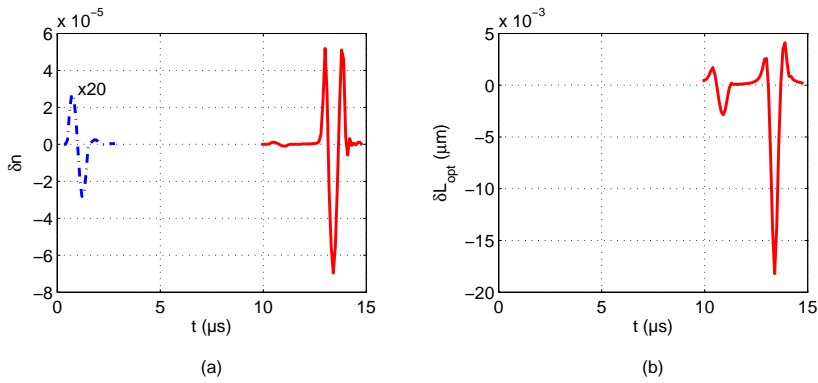


Fig. 2 (a) Refractive index modulation near the transducer surface (dashed line) and at the center (solid line). The small modulation around $11 \mu\text{s}$ is the part of the sound wave coming along the z -axis (z -pulse). The large one around $13.5 \mu\text{s}$ is the radial one (r -pulse). (b) Modulation of the optical length through the center of the transducer for the same pulse.

by a factor 50. This is not much less than the factor 75 expected for an isotropic medium with the same λ_s . Figure 2 also shows the behavior of the optical length through the center of the transducer. A first striking result is that the optical length is vanishingly small for almost all times, although the integration path crosses the wave at any time. This is because the positive and the negative parts of the wave cancel almost exactly. Only when the wave reaches the center is this no more true. The z -pulse seems to be magnified, but this is only a geometrical effect due to the fact that this part of the wave is almost plane and perpendicular to the z -axis. The ratio between the maximum amplitude of the optical length and the maximum amplitude of the index modulation is a characteristic length a ($a \simeq 0.28$ mm). It can be used to deduce the refractive index modulation, which is the quantity of interest, from the optical length, which is the measured quantity.

4 Presentation and discussion of some results

An example of observed optical signal $\delta L_{\text{opt}}(t)$ is shown in Figure 3-a. It was taken with a driving voltage $V_d = 200$ V at $T = 1.16$ K and a pressure 0.6 bar above $P_f(T)$. An order of magnitude of the sound amplitude at the transducer surface can be evaluated from the formula $\delta\rho/\rho = 2\pi d_{33} V_d / \lambda_s f_r$, where $d_{33} = 0.3$ nm/V is the piezoelectric constant at room temperature of the transducer ceramic, and $f_r \simeq 4$ is an order of magnitude of its reduction factor at low temperatures¹⁶. One finds $\delta\rho/\rho \simeq 2 \times 10^{-4}$, which can be converted to an acoustic pressure $\delta P = 54$ mbar using solid helium bulk modulus $B_s = 269$ bar.¹⁷ Thus the minimum pressure at the transducer surface is well above the melting pressure. Note that for low sound amplitudes ($\delta\rho/\rho < 10^{-2}$), the computation of δP using the bulk modulus instead of a non linear equation of state does not lead to a relative error larger than 10^{-2} .

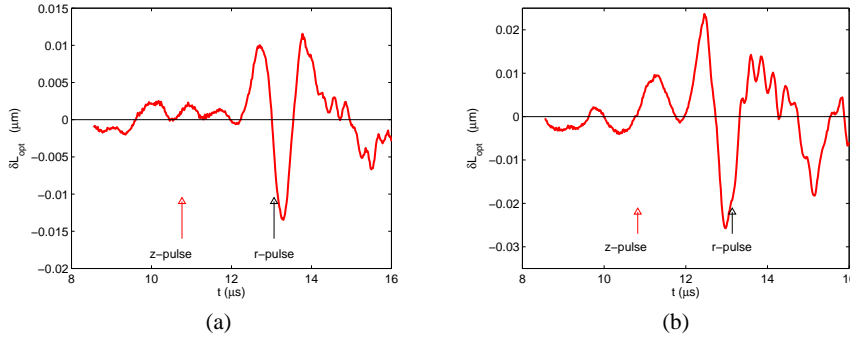


Fig. 3 Observed optical length modulation by focused sound pulses. Time origin is the beginning of the transducer oscillation which lasts 1 μ s. Arrows indicate the middle of expected z - and r -pulses. (a) driving voltage 200 V, initial offset from melting pressure 0.6 bar, pressure swing at focus -0.35 bar. (b) Same signal with parameter values 600 V, 0.1 bar, -0.9 bar respectively.

Comparison of the optical signal with Figure 2-b helps to identify the radial wave. The expected time of flight is indicated by the arrow labeled ‘ r -pulse’.

that in Figures 2 and 3 the origin of time is the beginning of the transducer oscillation. To get the time of flight for the middle of the sound pulse, half its duration is to be subtracted, namely $0.5\mu\text{s}$. The sound velocity at this particular pressure is determined using the scaling of c_{11} and c_{33} proposed by Maris¹. For this signal, the laser beam is thought to cross the focal region. In fact extensive scanning of the focal region along the x and z -axis with the laser beam was performed to locate the sound focus.

The shape of the r -pulse is qualitatively similar to the expected one. The width in time measured by the delay between the secondary maximums is close to the $1.0\mu\text{s}$ delay in Figure 2-b. There are several differences however. Some are parasitic effects. The high frequency modulation may be attributed to higher oscillation modes of the transducer which are found near 2.4 MHz and 3.6MHz. Oscillations before the expected z -pulse can be explained by the fact that the reference light beam is slightly perturbed by the wave emitted by the rim of the piezo-hemisphere. The distance between this rim and the reference beam is 4 mm and thus the sound wave reaches it in $7\mu\text{s}$. Concerning the r -pulse itself, the ratio of the main peak amplitude to the secondary maximums is much smaller than in the simulation. This could be due to an offset of the laser beam from the radial geometry or spatial averaging over the laser waist. Simulation shows that an offset of 0.1 mm would divide the peak by a factor 3.

There is not a clear evidence for the z -pulse. It is either absent or hidden by parasitic oscillations. Its weakening may be correlated to that of the r -pulse peak. Another possible explanation is that the initially well oriented mono-crystal has been broken and turned to a more or less isotropic polycrystal by the sound wave. As a matter of fact, during long measurement series for scanning the laser beam position, we occasionally observed evolution of the optical signal, generally a weakening of the pulse amplitude.

Let us come back to the intensity of the negative swing at focus. Using the value of a determined by the simulation ($a = 0.28\text{ mm}$), one gets an order of magnitude of the negative pressure swing from the formula $\delta P = \delta L_{opt} B_s / a(n - 1) \simeq -0.35\text{ bar}$. The initial pressure was 0.6 bar from the melting pressure, so that the minimum pressure does not reach the melting line. Figure 3-b shows another signal taken with a larger driving voltage (600 V) and starting closer to the melting line, $P - P_f = 0.11\text{ bar}$. The signal is clearly more distorted than in Figure 3-a. If one converts nevertheless the negative swing into pressure using the same formula quoted above, one gets $\delta P = -0.9\text{ bar}$. In that case, it appears that the pressure has crossed the equilibrium melting line by at least 0.8 bar.

Has helium remained in the solid phase? Had a liquid droplet nucleated at the focus, it would have expanded for a fraction of the sound half period at a velocity close to the sound velocity. Thus it would have reached a diameter on the order of $100\mu\text{m}$. Taking into account the refractive index difference between liquid and solid phases (about 0.0035), the liquid bubble would have created a jump in δL_{opt} as large as $0.35\mu\text{m}$. Also a large asymmetry would be found between positive and negative pressure swings. Neither of the two phenomena are observed and it can be concluded that transient melting did not occur.

5 Possible improvements and conclusions

A direct interferometric imaging has been developed¹⁸ to provide a map of δL_{opt} . It uses the same interferometer, but the laser is a pulsed laser and the detector a CCD camera. Images are taken for various t and reference phases. Then a map of $\delta\phi(t, x, z)$ can be computed for all the pixels in parallel. Beside providing a direct image of the sound pulse propagation in the crystal, inverse Abel transform will give access to the map of $\delta n(t, r, z)$, provided that it has a cylindrical symmetry. This should overcome the major shortcoming in the present experiment, namely the conversion from the measured δL_{opt} to the pressure swing δP at the focus. Since the observed signal differs from the simulation, a more direct way to compute the latter will be valuable. It will also avoid scanning the laser beam to locate the focus, which is both time consuming and harmful for the crystal. In order to view the focus and an extended portion of the x -axis, the lower part of the hemispherical transducer will be shortened by 1 mm or so. This new method will also help assessing whether the crystal is broken by repetitive sound pulses. If this is the case, it would be of interest to try to work with a polycrystal with grains smaller than λ_s . The medium will then be quasi-isotropic¹⁹. Whether the sound attenuation will be acceptable remains an open question. In the case monocrystals survive their repetitive stress, it would be more efficient to use a transducer with a shape conforming the wavesurface of the hcp crystal, or at least half of it. As depicted in reference¹⁰, it is an elongated bowl, nearly conical in the directions between z and x -axis. Finally using longer multi-oscillation excitation pulses will allow to reach oscillation amplitudes δP about 10 times larger. The more complex wave pattern will not be a problem if inverse Abel transform can be performed.

To summarize, it has been shown that interesting motivations exist to investigate solid helium below the melting pressure. Numerical simulations confirmed that sound waves can be efficiently focused in the anisotropic hcp crystal and provides a tool to investigate the metastable region below the melting curve. A first example of incursion in this domain has been reported, and perspectives exist to enlarge the explored domain.

Acknowledgements We acknowledge support from ANR, grant 05-BLAN-0084-01.

References

1. H. Maris, *J. Low Temp. Phys.* **155**, 290 (2009).
2. B. A. Fraass, P. R. Granfors and R. O. Simmons, *Phys. Rev.* **B39**, 124 (1989).
3. M. Boninsegni, A.B. Kuklov, L. Pollet, N.V. Prokof'ev, B.V. Svistunov and M. Troyer, *Phys. Rev. Lett.* **97**, 080401 (2006).
4. D.S. Greywall, *Phys. Rev.* **A3**, 2106 (1971).
5. A. F. Andreev and I. M. Lifshitz, *Zh. Eksp. Teor. Fiz* **56**, 2057 (1969). [*Sov. Phys-JETP* **29**, 1107 (1969)];
6. G.D. Mahan and H. Shin, *Phys. Rev.* **B74**, 214502 (2006).
7. See for instance S. Balibar and F. Caupin, *J. Phys.: Cond. Matter* **C15**, S75 (2003).
8. K.O. Keshishev, A.Y. Parshin, A.V. Babkin, *JETP* **53**, 362 (1981).

-
9. S. Balibar, H. Alles, A.Y. Parshin, *Rev. Mod. Phys.* **77**, 317 (2005)
 10. R.H. Crepeau and D.M. Lee *Phys. Rev.* **A6**, 516 (1972).
 11. K. Creath, *Progress in Optics*, vol.**26**, 349 (1988), E.Wolf editor (Elsevier)
 12. P. Debye, *Annalen der Physik* (Leipzig), vol.**29**, 755 (1909), formula (39)
 13. M.J.P. Musgrave, *Reports on Progress in Physics*, A.C. Strickland editor (The Physical Society, London 1969), Vol.XXII p.74.
 14. L D Landau, L. P. Pitaevskii, E.M. Lifshitz, A. M. Kosevich, *Theory of Elasticity* (Theoretical Physics, Vol 7), (Butterworth-Heinemann, third edition, 1986)
 15. R.H. Crepeau, O. Heybey, D.M. Lee and S.A. Stauss, *Phys. Rev.* **A3**, 1162 (1971).
 16. Some examples for barium titanate compounds can be found on the web site of Morgan Electro Ceramics (<http://www.morganelectroceramics.com/resources/technical-publications>), technical note TP-226
 17. E.R. Grilly, *J. Low Temp. Phys.*,**11** 33 (1973)
 18. F. Souris, J. Grucker, J. Dupont-Roc and Ph. Jacquier, *Appl. Optics*, accepted for publication 2010.
 19. H. Maris, S. Balibar, *J. Low Temp. Phys.* **160**, 5 (2010).